LA-UR-22-21063

Approved for public release; distribution is unlimited.

Title: Sesame Equation of State for Nickel

Author(s): Sjostrom, Travis

Intended for: Report

Issued: 2022-02-18 (rev.1)

Los Alamos
NATIONAL LABORATORY

Los Alamos National Laboratory, an affirmative action/equal opportunity employer, is operated by Triad National Security, LLC for the National Nuclear Security Administration of U.S. Department of Energy under contract 89233218CNA000001. By approving this article, the publisher recognizes that the U.S. Government retains nonexclusive, royalty-free license to publish or reproduce the published form of this contribution, or to allow others to do so, for U.S. Government purposes. Los Alamos National Laboratory requests that the publisher identify this article as work performed under the auspices of the U.S. Department of Energy. Los Alamos National Laboratory strongly supports academic freedom and a researcher's right to publish; as an institution, however, the Laboratory does not endorse the viewpoint of a publication or guarantee its technical correctness.

Sesame Equation of State for Nickel

Travis Sjostrom
Theoretical Division, Los Alamos National Laboratory, Los Alamos, New Mexico 87545
(Dated: February 18, 2022)

A new Sesame equation of state table for nickel has been created and released for testing. The material ID is 83103. Of note the new table incorporates a magnetic contribution based on specific heat data and a melt curve based on experimental data to 100 GPa.

INTRODUCTION

A new Sesame equation of state (EOS) table for nickel has been created and released for testing with the material ID 83103. This table is intended as complete range table. The motivation was to generate a more accurate table based on newer modeling methods and where newer experimental data was available than was for the previous table. While there is some suggestion for a very high pressure solid-solid phase change, that is not incorporated in this table and assumes FCC as the only solid phase. The table has been constructed as a pseudo-multiphase EOS, with the nuclear model distinguishing the solid and liquid regimes. We have also included a magnetic contribution to bring the EOS into alignment with experimental data. The reference density for the table is taken to be 8.91 g/cm^3. A pressure-temperature diagram of the EOS is shown in figure 1 indicating the melting and the principal Hugoniot. Other nickel equations of state in the literature include Refs. 1 and 2.

EOS CONSTRUCTION AND RESULTS

As is the general approach our EOS is based on evaluation of the Helmholtz free energy in density, ρ, and temperature, T, space, and is written with the following decomposition [3]

$$F(\rho, T) = E_{\rm cc}(\rho) + F_{\rm ion}(\rho, T) + F_{\rm el}(\rho, T) \ , \qquad (1)$$

where $E_{\rm cc}$ is the cold curve contribution, $F_{\rm ion}$ is the thermal contribution for the ions, and $F_{\rm el}$ is the contribution from the electron excitations.

For the cold curve we make use of a finite strain equation of state (see Eq. 19 of Ref. 3). Here we only use the 4 parameters for the cold curve reference density, bulk modulus, the pressure derivative of the bulk modulus, and the first expansion coefficient C_1. For low density we match to a Lennard-Jones equation of state below a density of 8.375 g/cm^3, and for high density which match to a Thomas-Fermi-Dirac equation of state above 26.73 g/cm^3. Again for formulary see Ref. 3. Exact parameters for the cold curve and other models are in the attached input file below.

For $F_{\rm ion}$ we use the Johnson model [4], version 2. This model allows use to generate the pseudo-multiphase EOS with separate liquid and solid regions. This model is essentially a Debye model below melt and interpolative to an ideal gas above melt. Both regions are dependent on a single function for the Grüneissen parameter, Γ, for which we use Eq. 30 of Ref. 3. The Γ reference density is set at 9.1256 g/cm^3, and then the calculated Debye temperature from the model is $\Theta_D = 425$ K. The Johnson model uses the Lindemann equation to calculate the melt. Here, however, we have changed that to use the experimentally derived Simon-Glatzel fit to the melting data [5]

$$T_{\rm melt} = 1727 \times \left[\frac{P_{\rm melt}}{17} + 1\right]^{1/2.5} \ , \qquad (2)$$

where $T_{\rm melt}$ is in K and $P_{\rm melt}$ is in GPa. This fit is only over experimental data up to 100 GPa, though we use it from ambient pressure through the highest densities of the table. Below ambient pressure, roughly below $\rho = 8.3$ g/cm^3, we use the Lindemann formula.

For $F_{\rm el}$ we calculate the thermal electron free energy by using the Tartarus average atom code [6]. As with a Thomas-Fermi-Dirac (TFD) average atom calculation a single ion is solved embedded in a plasma. However in Tartarus the Kohn-Sham electron orbitals are calculated instead of using the semi-classical TFD electron density. We also included an additional magnetic contribution which uses an empirically based model for the

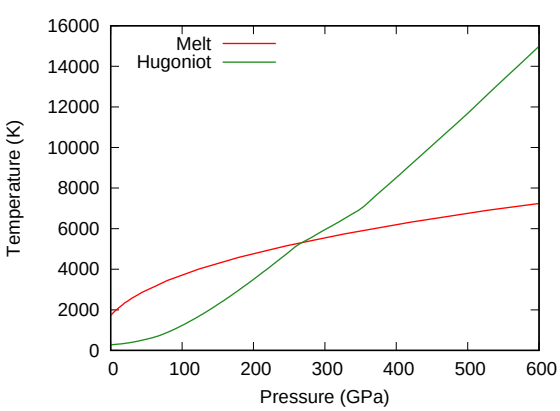

FIG. 1: Phase diagram for nickel EOS 83103, showing melt and the principal Hugoniot.

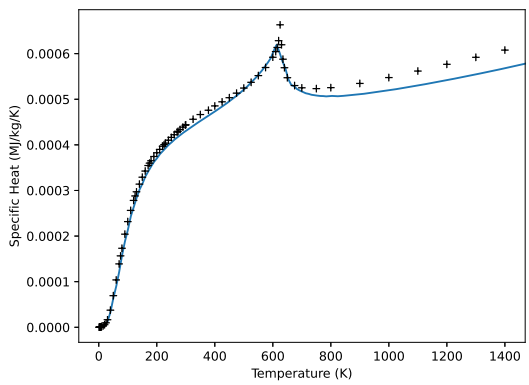

FIG. 2: Isobaric specific heat C_P of nickel below the melting temperature [8].

specific heat [1, 7]

$$C_{V,\mathrm{mag}}(T) = K_A T^{3/2}/(r_A T_C - T) \ , \quad T < T_C \ , \qquad (3)$$

$$C_{V,\mathrm{mag}}(T) = K_B/(T - r_B T_C)^2 \ , \quad T > T_C \ , \qquad (4)$$

where $T_C = 631$ is the Curie temperature in K, and $K_A = 1.98 \times 10^{-6}$, $K_B = 1.31$, $r_A = 1.3$, $r_B = 0.816$ with $C_{V,\mathrm{mag}}$ in MJ/kg/K. $C_{V,\mathrm{mag}}$ is then integrated to give the interanl energy and entropy terms. It is of note that this model assumes no dependence with the volume.

The combination of using a Tartarus based table and the magnetic contribution allows us to find very good agreement for the specific heat of nickel with experiment as shown in figure 2. The values in the plot are the recommended values of Desai [8], based on available data on nickel through 1984. The value of C_P does rise higher than the EOS for temperatures above 800 K, and this may indicate that anharmonic contributions are needed in the ion model which go beyond the Debye model we have used.

Other isobaric data the EOS was fit to include the thermal expansion and the enthalpy, which are both shown in figure 3. Both sets show good agreement for the solid and liquid phases as well as the melt transition temperature. Though the data is a little scattered for the liquid thermal expansion, a best fit would indicate a slightly lower density than what the EOS yields.

In the top panel of figure 4 we have plotted the EOS 300 K pressure isotherm along with recent diamond anvil cell data [12], which shows good agreement to 156 GPa. In the bottom panel we have plotted the results for the Hugoniot with all available experimental results [13], which reach to nearly two times compression.

Finally, we note the EOS finds the critical point at $\rho = 1.00$ g/cm^3, $T = 9850$ K, and $P = 0.65$ GPa, which compares relatively well with experiment [22] and molecular dynamics simulations [23].

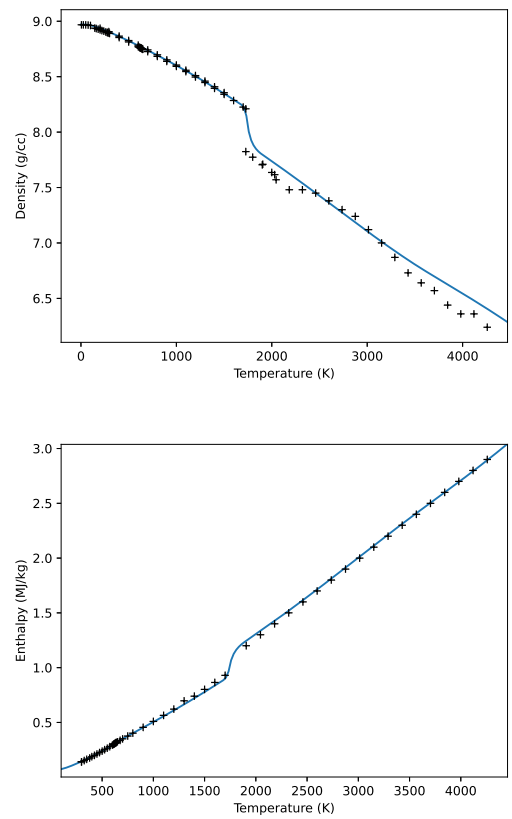

FIG. 3: Nickel isobaric results in the solid and liquid phases for (top) the thermal expansion [9–11] and (bottom) the enthalpy [8, 11] to over 4000 K.

The EOS was generated using the LANL OpenSesame code. Determination of the parameters was completed by using particle swarm optimization against the data shown in figures 2-4. The melt curve was enforced to be Eq. 2 in the jdjnuc model of OpenSesame, as was noted earlier. This was done in a local modification of OpenSesame and not available in the code. The magnetic model has been implemented in the master branch of OpenSesame since Feb. 2022. Those parameters and all other are in the input file which is below. The Tartarus table for nickel, along with others, is being made available in the LANL eos-developmental space.

[1] G. Kerley, Sandia Report, SAND 2003-3784 (2003)
[2] I. V. Lomonosov, V. K. Gryaznov, Contrib. Plasma Phys. 56, 302 (2016)
[3] T. Sjostrom, in *Shock Phenomena in Granular and Porous Materials. Shock Wave and High Pressure Phenomena*, edited by T. Vogler and D. Fredenburg (Springer, Cham. 2019), pp. 3-38
[4] J. D. Johnson, High Pressure Research 6, 277 (1991)

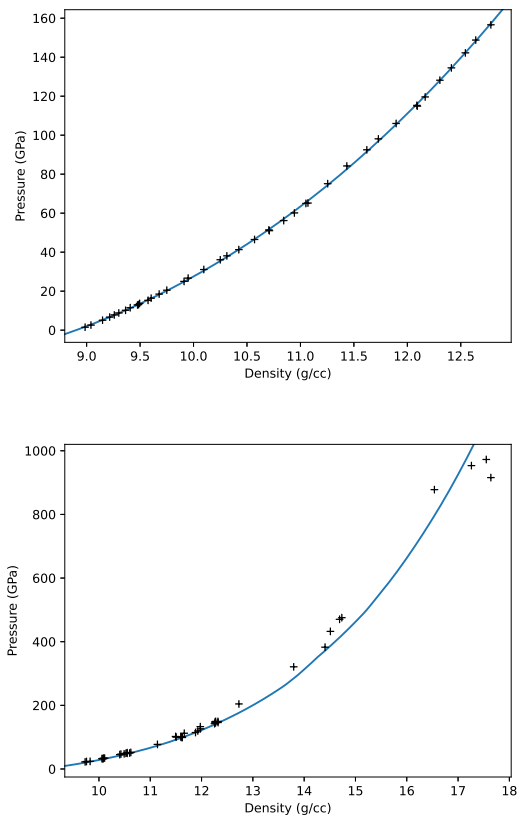

FIG. 4: Nickel pressure-density results for (top) the 300 K isotherm [12] and for (bottom) the principal Hugoniot [13].

[5] S. Boccato, R. Torchio, I. Kantor, G. Morard, S. Anzellini, R. Giampaoli, R. Briggs, A. Smareglia, T. Irifune, S. Pascarelli, Journal of Geophysical Research: Solid Earth 122, 9921 (2017)

[6] N.M. Gill, C.E. Starrett, High Energy Density Physics 24, 33 (2017)

[7] D. J. Andrews, J. Phys. Chem. Solids 34, 825 (1973)

[8] P. D. Desai, International Journal of Thermophysics, 8, 763 (1987)

[9] CINDAS recommended values. Retrieved from CINDAS LLC *Thermophysical Properties of Matter Database* (TPMD). Version 10.0 at http://cindasdata.com/ (sourced Aug. 2021)

[10] R. N. Abdullaev, Y. M. Kozlovskii, R. A. Khairulin, S. V. Stankus, Int J Thermophys 36, 603 (2015)

[11] R. S. Hixson, M. A. Winkler, and M. L. Hodgdon, Phys. Rev. B 42, 6485 (1990)

[12] A. Dewaele, M. Torrent, P. Loubeyre, and M. Mezouar, Phys. Rev. B 78, 104102 (2008)

[13] A. V. Bushman, I. V. Lomonosov and K. V. Khishchenko, *Shock Wave Database*, http://www.ihed.ras.ru/rusbank (sourced Aug. 2021)
Note: Original references are [14–21]

[14] J. M. Walsh, M. H. Rice, R. G. Mcqueen, F. L. Yarger, Phys. Rev. 108, 196-216 (1957)

[15] R. G. McQueen, S. P. Marsh, J. Appl. Phys. 31, 1253-1269 (1960)

[16] S. B. Kormer, A. I. Funtikov, V. D. Urlin, A. N. Kolesnikova, Zh. Eksp. Teor. Fiz. 42, 686-701 (1962) [in Russian] (Sov. Phys. - JETP 15, 477-478 (1962))

[17] L. V. Al'tshuler, A. A. Bakanova, R. F. Trunin, Zh. Eksp. Teor. Fiz. 42, 91-104 (1962) [in Russian] (Sov. Phys. - JETP 15, 65-74 (1962))

[18] W. H. Isbell, F. H. Shipman, A. H. Jones, General Motors Corp., Mat.Sci.Lab. Report MSL-68-13, (1968)

[19] S. P. Marsh (Ed.), *LASL Shock Hugoniot Data*, (Univ. California Press, Berkeley, 1980)

[20] L. V. Al'tshuler, A. A. Bakanova, I. P. Dudoladov, E. A. Dynin, R. F. Trunin, B. S. Chekin, Zh. Prikl. Mekh. Tekhn. Fiz. 2, 3-34 (1981) [in Russian] (J. Appl. Mech. Techn. Phys. 22, 145 (1981))

[21] R. F. Trunin, G. V. Simakov, Yu. N. Sutulov, A. B. Medvedev, B. D. Rogozkin, Yu. E. Fedorov, Zh. Eksp. Teor. Fiz. 96(9), 1024-1038 (1989) [in Russian] (Sov. Phys. - JETP 69(3), 580-588 (1989))

[22] D. N. Nikolaev, V. Ya. Ternovoi, and A. A. Pyalling, AIP Conference Proceedings 620, 59-62 (2002)

[23] C. Cheng, X. Xu, International Journal of Thermophysics 28, 9 (2007)

in.Ni - the input file for nickel including the temperature grid job for capturing the specific heat accurately.

```
&job
 job_type="grid" /

&grid
 grid_type="temperature"
 grid_change="delete"
 grid_limit_lo=0
 grid_limit_hi=800
 grid_temperature_units='K'
/


&job
 job_type="grid" /

&grid
 grid_type="temperature"
 grid_change="insert"
 grid_limit_lo=0
 grid_limit_hi=800
 grid_size=33
 grid_spec="lin"
 grid_temperature_units='K' /

&job
   job_type='neweos'
   resultlib_path='./'/

&neweos
   material_number=83103
   material_name='nickel'
   author='Travis Sjostrom'
   references=''
   atomic_number=28
   atomic_weight=58.693
   reference_density=8.91
   ifstandard=.false.
   energy_shift=0.0

   !!!! cold curve
   cold_model='finite_strain'
   cold_bulk_modulus=188.941
   cold_dbdp=4.9
   cold_density=9.0230
   fs_coeff=-25
   lower_compression_cutoff=0.940
   upper_compression_cutoff=3.0
   lennard_jones_exponent=1.25
   cohesive_energy_kc=100.0

   !!!! nuclear contribution
   nuclear_model='gjdjnuc'
   liquid_multiplier=1.02
   meltwidthjdjnuc=0.02
   gruneisen_option=7
   gamma_reference_density=9.1256
   reference_gamma=2.05
   gamma_at_zero=1.0
   gamma_at_infinity=1.0
   dgamma_left=-2.05
   dgamma_right=-2.05
   melt_model='function'
   melt_option='other'
   initial_melt_density=8.22
   initial_melt_temperature=1728

   !!!! electronic contribution
   electron_model='electron_material'
   electron_material_number=92028
   magnetic_model='CV'
   mag_params=1.98d-6 1.3 1.31 0.816 631.0
 /
```